RSC Advances

PAPER

View Article Online
View Journal | View Issue

Cite this: *RSC Adv.*, 2021, **11**, 31663

Sc/C codoping effect on the electronic and optical properties of the TiO_2 (101) surface: a first-principles study

Dongxiang Li,[ab] Ruiqin Li,[b] Fanjin Zeng,[ab] Shuyi Wang,[c] Wanjun Yan,[d] Mingsen Deng *[ce] and Shaohong Cai*[e]

Extension of the light absorption range and a reduction of the possibility of the photo-generated electron–hole pair recombination are the main tasks to break the bottleneck of the photocatalytic application of TiO_2. In this paper, we systematically investigate the electronic and optical properties of Sc-doped, C-doped, and Sc/C-codoped TiO_2 (101) surfaces using spin-polarized DFT+U calculations. The absorption coefficient of the Sc/C-codoped TiO_2 (101) surfaces were enhanced the most compared with the other two doped systems in the high energy region of visible light, which can be attributed to the shallow impurity states. Furthermore, we studied the optical absorption properties with the change of the impurity concentration. The Sc/C-codoped TiO_2 (101) surface with 5.56% impurity concentration exhibited optimal photocatalytic performance in the visible region. These results may be helpful for designing the high-performance of the photocatalysts by doping.

Received 28th July 2021
Accepted 7th September 2021

DOI: 10.1039/d1ra05756a

rsc.li/rsc-advances

1 Introduction

Transition metal oxides have attracted tremendous attention due to its wide applications in photocatalysis, electronic devices, solar cells and heterogeneous catalysis in the past few decades.[1–13] TiO_2 has many advantages, including non-toxicity, inexpensiveness, highly oxidative property, and resistance to photo corrosion. However, TiO_2 has a band gap of 3.2 eV,[14] resulting in a light response in the UV range. In addition, the recombination of photo-excited electrons and holes can reduce the photocatalytic performance of the material. Therefore, the extension of the light absorption range and improvement of the quantum efficiency are regarded as two main approaches to improve the photocatalytic activity of TiO_2.

Recent studies have shown that transition metal (TM)[15–19] and non-metal atoms doping[20–23] are a feasible and efficient way to enhance the photocatalytic performance of TiO_2. Nevertheless, the TM doping is deemed unstable and can introduce localized impurity states, which increase the recombination rate of photo-generated electron–hole pairs.[24–26] On the other hand, it has been found that the electronic and optical properties of TiO_2 have been remarkably regulated by doping C atoms. Owing to the presence of impurity states (C-2p states) in the band gap, the excitation energy of electrons in TiO_2 is greatly reduced, which is responsible for the red-shift of the optical absorption edge. However, these impurity states in the band gap can also serve as carrier recombination centers that significantly reduce the carrier mobility.

Compared to single carbon doping, the codoping of carbon and the transition metal atom have gained particular attention because of the remarkably enhanced photocatalytic activity for TiO_2. A large number of TiO_2 codoped with carbon and transition metal atoms have been successfully prepared, which possess the visible-light photocatalytic activity, owing to the extension of the absorption into the visible-light region. Liu *et al.* have shown that C/V co-doped TiO_2 exhibits excellent visible light activity,[27] where the improved photocatalytic activity can be attributed to the synergistic effects between vanadium and carbon. Cai *et al.* have synthesized Mn/C-codoped TiO_2 by modified sol–gel method,[28] and the Mn/C-codoped TiO_2 has high photocatalytic activities for the decolorization of methyl orange aqueous solution.

In order to understand the underlying mechanism for the significantly enhanced photocatalytic activity, many theoretical investigations have focused on codoped TiO_2 by employing density functional theory calculations. The reduced band gap for TiO_2 was considered to be responsible for the enhanced photocatalytic activity. Morgade *et al.* have observed that the band gap of Pt/C-codoped TiO_2 decreases that due to the introduction of impurity states.[29] Li *et al.* presented that the Cr/

[a]*College of Big Data and Information Engineering, Guizhou University, Guiyang 550025, China. E-mail: deng@gznc.edu.cn; caish@mail.gufe.edu.cn*

[b]*College of Mathematics and Physics, Anshun University, Anshun 561000, China*

[c]*Guizhou Provincial Key Laboratory of Computational Nano-material Science, Guizhou Education University, Guiyang 550018, China*

[d]*College of Electronic and Information Engineering, Anshun University, Anshun 561000, China*

[e]*School of Information, Guizhou University of Finance and Economics, Guiyang 550025, China*

C-codoped system displays better visible light absorption than the mono-doped system due to the narrowing of the band gap.[30] Chen *et al.* found that the Ni/C-codoped TiO_2 has the smallest direct band gap and shows a red-shift of the absorption band edge.[31] These results indicate that carbon and transition metal codoping is one of the most effective approaches to enhance optical performance.

Recently, Nasir *et al.* have synthetized a Sc/C-codoped TiO_2 catalyst and suggested that the recombination rate of the photo-generated electron–hole pairs decrease with increasing Sc concentration,[32] where the enhanced photocatalytic performance can be ascribed to the increase of the surface area and synergistic effect between Sc and C impurities. So far, however, the origin of the improved photocatalytic activity for Sc/C-codoped TiO_2 is not clear. In this paper, we studied the electronic structures and photocatalytic properties of Sc- or/and C-doped TiO_2 (101) surfaces systematically. The Sc/C codoped system could effectively enhance the separation rate of photo-generated carriers because of lattice distortion and the band gap narrowing caused by the synthesis effect. When the impurity concentration of Sc and C reached 5.56%, the doped system showed better optical absorption performance in the visible region. Our calculated results in this paper explain the experimental phenomena well, and provide a reliable theoretical basis for the preparation of efficient photocatalysts.

2 Computation methods and models

Density functional theory (DFT) calculations were carried out using the projector augmented wave (PAW) method, as implemented in the Vienna *Ab initio* Simulation Package (VASP) code.[33,34] The generalized gradient approximation (GGA) with Perdew–Burke–Ernzerhof (PBE) functional[35] was chosen for geometry relaxation and total energy calculations. The atomic position was relaxed until the convergence criteria for the energy and force were smaller than 1×10^{-5} eV and 0.01 eV $Å^{-1}$, respectively. The valence atomic configurations used in the calculation contained Ti for $3p^6 3d^2 4s^2$, O for $2s^2 2p^4$, Sc for $3s^2 3p^6 3d^1 4s^2$ and C for $2s^2 2p^2$. To get an accurate electronic structure for anatase TiO_2, the DFT+U method was also used in the electronic structural calculations.

The linear optical absorption spectra were described by the frequency-dependent complex dielectric function $\varepsilon(\omega)$, $\varepsilon(\omega) = \varepsilon_1(\omega) + i\varepsilon_2(\omega)$, where $\varepsilon_1(\omega)$ and $\varepsilon_2(\omega)$ were the real and imaginary parts of the dielectric function, and ω was the photon frequency. Based on the dielectric function, the absorption coefficient $\alpha(\omega)$ could be obtained by the following equation:[36]

$$\alpha(\omega) = \sqrt{2}\omega\left[\frac{\sqrt{\varepsilon_1^2 + \varepsilon_2^2} - \varepsilon_1}{2}\right]^{1/2} \quad (1)$$

For the bulk anatase structure, the calculated lattice parameters were $a = 3.803$ Å and $c = 9.770$ Å, which were in good agreement with previous experimental results and theoretical predictions.[37,38] Our model for the TiO_2 (101) surface was constructed on the basis of 18 atomic layers with a vacuum space of 18 Å. For geometry relaxation, the six atomic layers at the bottom of the slab are fixed, while the other atoms were allowed to relax. The plane-wave cut-off energy was set to 500 eV. The k point grids of the geometry relaxation and electronic properties calculations were used for $2 \times 4 \times 1$ and $3 \times 5 \times 1$, respectively. The doping model was constructed using a $2 \times 2 \times 1$ TiO_2 (101) surface, as shown in Fig. 1. The marked number above the atom represents the coordination number of the corresponding atom. Various defects related to the Sc- or/and C-doped TiO_2 (101) surfaces were considered, such as interstitial Sc atom (Sc@in), substitutional Sc for Ti (Sc@Ti), substitutional C for O with (C@O), and interstitial C atom (C@in). Here, Sc at the Ti site and C at the interstitial site were considered (Sc@Ti&C@in) for the Sc/C-codoped TiO_2 (101) surface. Two doping concentrations of 1.39 and 2.78 at% were involved for the Sc- or/and C-doped TiO_2 (101) surface. In order to study the effects of the doping concentration on the TiO_2 (101) surface systematically, two kinds of surface models ($2 \times 1 \times 1$ and $2 \times 3 \times 1$ TiO_2 (101) surfaces) had been constructed. The k point grids of $2 \times 7 \times 1$ ($2 \times 2 \times 1$) and $3 \times 9 \times 1$ ($4 \times 4 \times 1$) were used for geometry relaxation and electronic property calculations for the $2 \times 1 \times 1$ ($2 \times 3 \times 1$) surface, respectively. The doping concentrations of Sc or/and C doping in the $2 \times 1 \times 1$ ($2 \times 3 \times 1$) surface were about 2.78 (0.93) and 5.56 (1.86) at%. The electronic structures and absorption spectra were post-processed by VASPKIT code.[39]

The surface energy (E_{surf}) of the pure TiO_2 (101) surface was calculated by:

$$E_{surf} = (E_{slab} - NE_{bulk})/(2A) \quad (2)$$

where E_{slab} was the total energy of the slab and E_{bulk} was the energy of each TiO_2 formula units in the bulk TiO_2. N is the number of TiO_2 formula units contained in the slab. A was the surface area of the slab. The surface energy of the model was

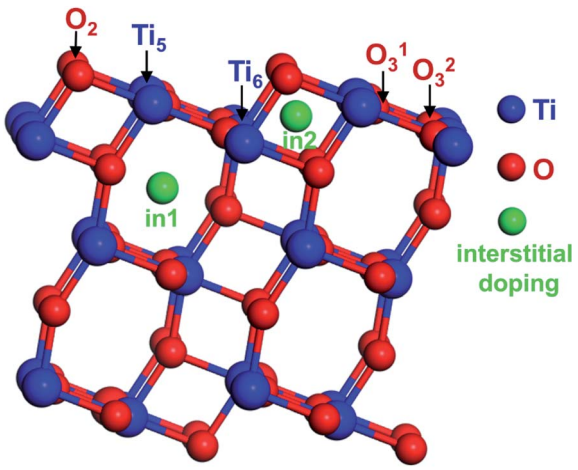

Fig. 1 The $2 \times 2 \times 1$ TiO_2 (101) surface shows the doped sites. There are seven doped positions of the Sc and C atoms: 2-fold coordinated O atom (O_2), two 3-fold coordinated O atom (O_3^1 and O_3^2), 5-fold coordinated Ti atom (Ti_5), 6-fold coordinated Ti atom (Ti_6), and two kinds of interstitial site doping (in1 and in2).

evaluated to be 0.43 J m^{-2}, which was in good agreement with the previous calculations.[40,41]

3 Results and discussion

3.1 Structure and defect formation energies

To investigate the thermal stability of those impurities in the TiO_2 (101) surface, the defect formation energies (E_{for}) of the Sc- or/and C-doped systems were calculated according to the equation:

$$E_{for} = E_d - E_p + m(\mu_O - \mu_C) + n(\mu_{Ti} - \mu_{Sc}) - k\mu_i \quad (3)$$

where E_d and E_p were the total energies of the doped and pure TiO_2 (101) surface. The terms m, n, and k refer to the number of impurity atoms. The chemical potential of Sc was obtained by the bulk Sc metal. The chemical potentials of μ_{Ti} and μ_O were determined by synthesis conditions (Ti-rich or O-rich), and should satisfy the relations of $\mu_{Ti} + 2\mu_O = \mu_{TiO2}$. Under the O-rich condition, μ_O was derived from the energy of an O_2 molecule. In the case of the Ti-rich environment, μ_{Ti} can be obtained from the bulk Ti metal. The μ_C was the chemical potential of C that was obtained from the relationship, $\mu_C + 2\mu_O = \mu_{CO2}$. The formation enthalpy of the pure TiO_2 (101) surface was predicted to be −10.96 eV, in good agreement with the value (−9.6 ± 0.8 eV) reported in ref. 42.

The defect formation energies of several typical doping structures are listed in Table 1. It was noted that the formation energies of the Sc-doped TiO_2 (101) surface were negative, as shown in Table 1, indicating that the substitution of Sc for Ti was exothermic. Moreover, the formation energies of substitutional C for O were much larger than that of the Sc-doped TiO_2 (101) surface under both Ti-rich and O-rich conditions, which indicated that the C-doped TiO_2 (101) surface was correspondingly difficult to be synthesized. In addition, the Ti atom was easier to be substituted for the Sc atom, while the O atom was easier to dope into a lattice as an interstitial atom under both O-rich and Ti-rich conditions. This means that Sc@Ti^5&C@in2 is most likely to be synthesized when the Sc atom and C atom are simultaneously doped. Therefore, our calculations indicate that the Sc/C-codoped TiO_2 (101) surface is more easily synthesized under an O-rich condition in experiment because the negative formation energy is led by the compensated effect. Due to the low formation energy, Sc@Ti^5, C@in2, and Sc@Ti^5&C@in2 were adopted in further investigation.

Table 1 The defect formation energies of Sc- or/and C-doped TiO_2 (101) surface

Model		E_{for} (eV) O-rich	E_{for} (eV) Ti-rich
Mono-doped	Sc@in1	−3.03	−3.03
	Sc@in2	−2.81	−2.81
	Sc@Ti^5	−9.11	−3.43
	Sc@Ti^6	−8.90	−3.22
	C@in1	9.02	9.02
	C@in2	8.79	8.79
	C@O^2	13.71	10.87
	C@O_3^1	13.92	11.07
	C@O_3^2	14.27	11.43
Co-doped	Sc@Ti^5&C@in2	−2.51	3.17

Table 2 Average bond lengths of the pure and Sc- or/and C-doped TiO_2 (101) surfaces after geometry optimization

Bond length (Å)	Pure	Sc-doped	C-doped	Sc/C-codoped
Ti–O	1.941	1.933	2.035	1.987
Sc–O	—	2.047	—	2.071
C–O	—	—	1.312	1.315
C–Ti	—	—	2.086	2.044

The geometry structures of the pure and Sc- or/and C-doped TiO_2 (101) surfaces were relaxed by the DFT+U calculations. The average bond lengths are shown in Table 2 and Fig. 2. We found that five Sc–O bonds are formed by the substitutional Sc for Ti in the TiO_2 (101) surface (Fig. 2(b)). Because the atomic radius (1.45 Å) of the Ti atom was smaller than that of the Sc atom (1.64 Å), the Sc–O bond length was longer than that of the Ti–O bond in pure TiO_2. Meanwhile, the variation of the bond length also caused a slight change of the O–Ti–O bond angle (from 153° to 155°). For the C-doped TiO_2 (C@in2) TiO_2 (101) surface (Fig. 2(c)), the length of the C–Ti bond was longer than the original Ti–O bond, which can be attributed to the larger atomic radius (C: 0.91 Å > O: 0.65 Å). Moreover, the length of the Ti–O bond (2.035 Å) clearly increased with respect to the original value of 1.941 Å. In particular, the bond angle of O–Ti–O (154°) clearly shows the phenomenon of the bond angle reversal and enlargement. The Ti–O bond length of the Sc/C-codoped TiO_2 (Sc@Ti^5&C@in2) surface (Fig. 2(d)) was between that of the Sc-doped model and C-doped model, which could be explained by the synergistic effect between the Sc atom and C atom. These changes show that the doping can bring about the apparent lattice deformation, which may change the dipole moments and affect the separation of the electron–hole pairs.[43–45]

3.2 Electronic structures and photocatalytic activity

The band structures and density of states (DOS) of the bulk TiO_2 and TiO_2 (101) surface were calculated by DFT+U method to gain the accurate band gap shown in Fig. 3. It was found that bulk TiO_2 was an indirect band gap semiconductor. The calculated band gap was 3.18 eV with a U value of 7.0 eV, which was very close to previous theoretical[46] and experimental[47] results. Thus, the electronic structures of the TiO_2 (101) surface also were calculated for U_{eff} = 7.0 eV in Fig. 3(b). Because the valence band maximum (VBM) and the conduction band minimum (CBM) were both located at the G point, the TiO_2 (101) surface became a direct band gap semiconductor. The band gap of this slab became 2.99 eV due to the presence of the surface states, which was consistent with the other theoretical results (3.05 eV).[48] In addition, the conduction bands (CB) of the bulk TiO_2 and TiO_2 (101) surface were mainly contributed by Ti-

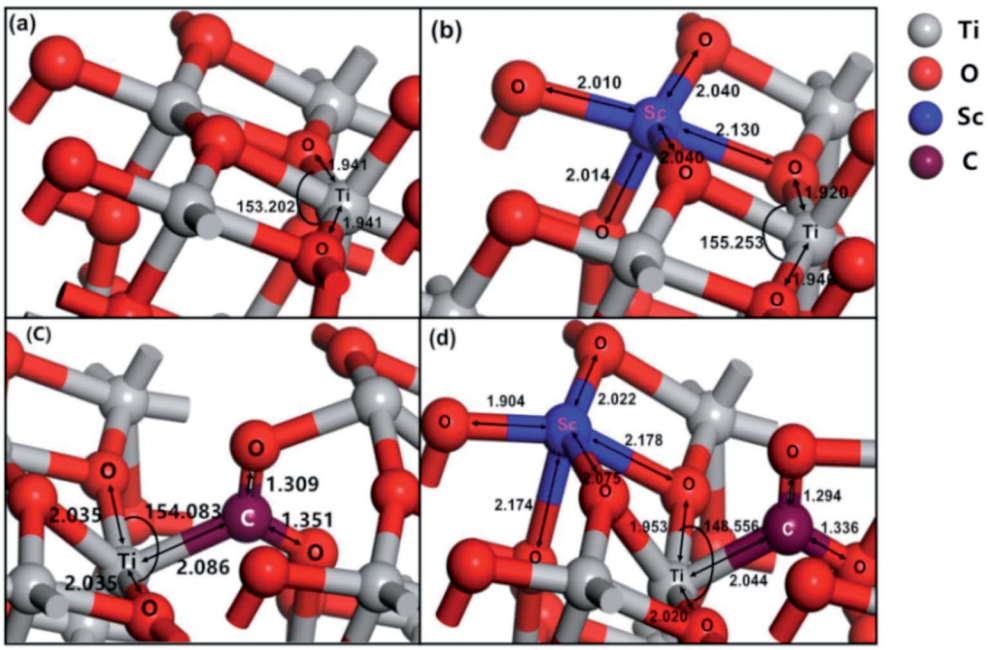

Fig. 2 Optimized geometrical configurations and partial bonds length for (a) pure, (b) Sc-doped, (c) C-doped, and (d) Sc/C-codoped TiO_2 (101) surfaces.

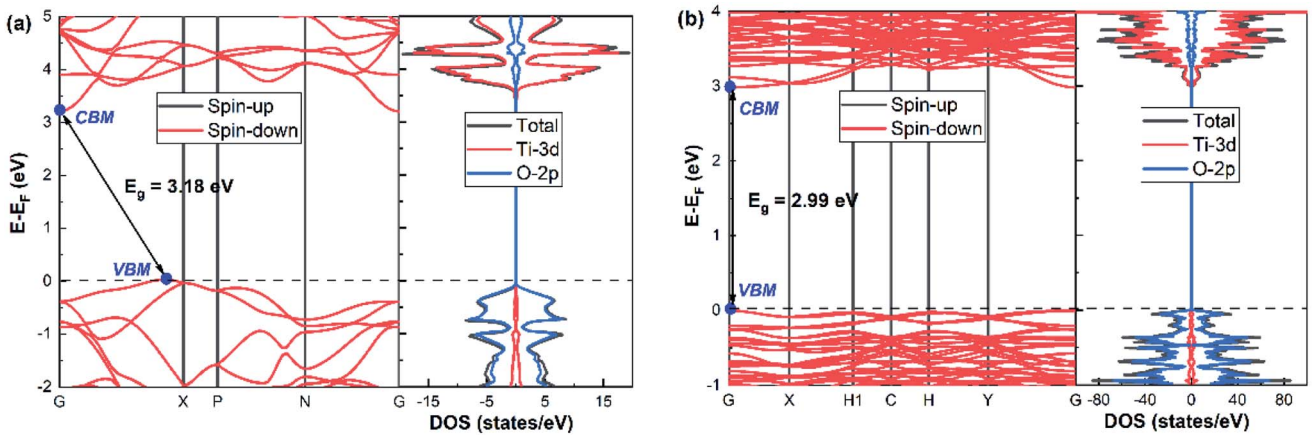

Fig. 3 The band structures and density of states for the 6-atom bulk TiO_2 (a) and 72-atom TiO_2 (101) surface (b). The black solid lines represent the Fermi level that is set to zero.

3d states, while the valence bands (VB) were mainly composed of O-2p states. In addition, a mild hybridization between the Ti-3d states and O-2p states could be observed near the CBM of the TiO_2 (101) surface.

In order to further explore the effects of Sc or/and C doping on the electronic properties of the TiO_2 (101) surface, the band structures and DOSs were plotted in Fig. 4. It was found that the positions of the CBM and VBM of the Sc-doped TiO_2 (101) surface upshifted steadily compared to the pure TiO_2 (101) surface, and the band gap decreases by about 0.03 eV, as shown in Fig. 4(a). Interestingly, the Fermi level of the Sc-doped TiO_2 (101) surface pinned the partial VB (Fig. 4(a′)), indicating semimetal properties. Since the electrons of the Sc atom are less than that of the Ti atom, the O-2p state will not be filled and a hole state will be introduced near the Fermi level. Therefore, electrons could be excited to the empty bands through a small excitation energy, which can increase the absorption in the low energy region of visible light. In addition, the impurity band is not introduced into the band gap of the Sc-doped system. It could be understood by the quite close size of Sc^{3+} and Ti^{4+}, which means that the substitution of Sc^{3+} in the site of Ti^{4+} is relatively facile and stable. The similar phenomenon has been reported by relevant literature.[49,50]

Compared to the pure TiO_2 (101) surface, the positions of the CBM and VBM had a sharp decrease (1.03 eV and 1.01 eV) for the C-doped TiO_2 (101) surface (Fig. 4(b)). It could be observed

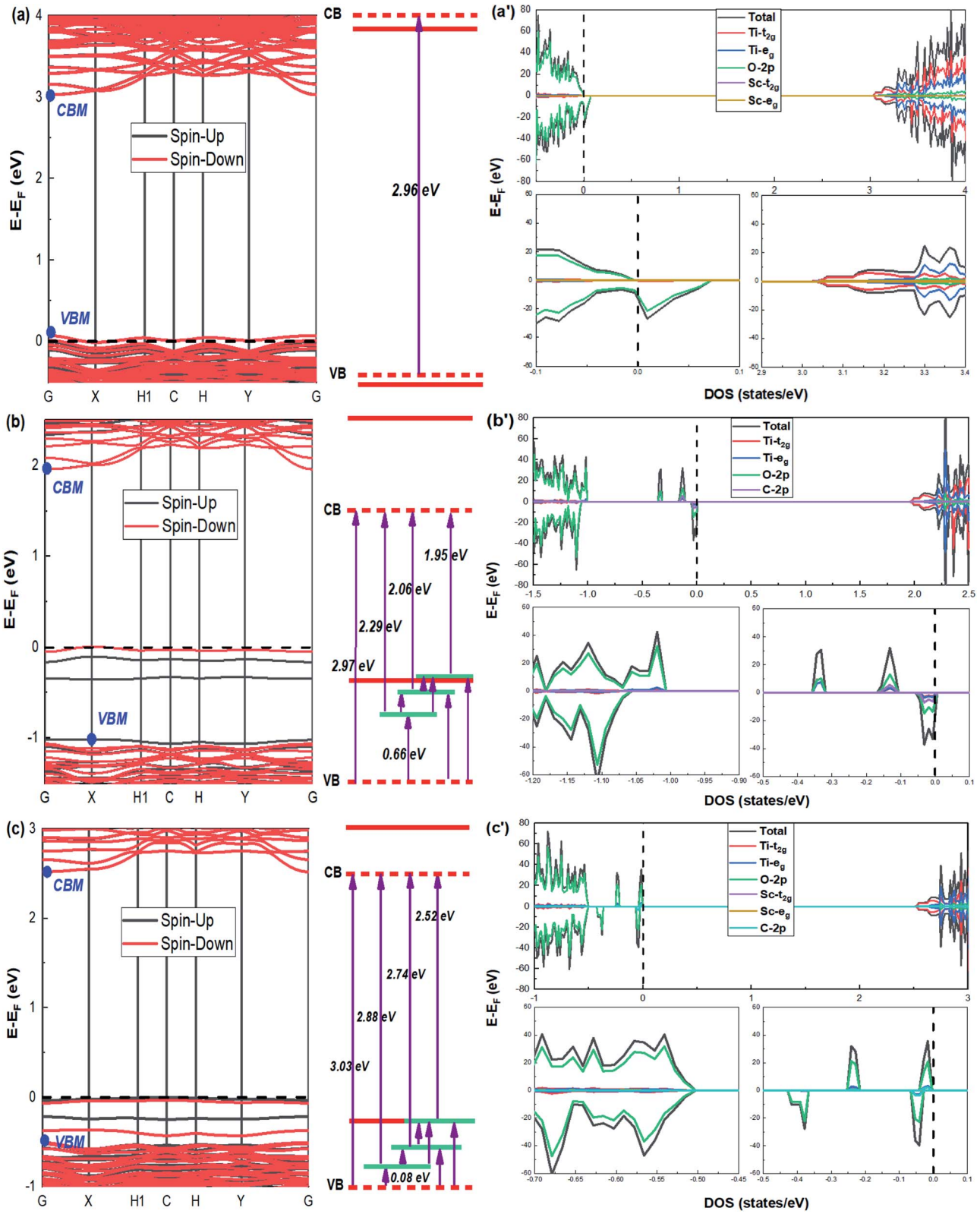

Fig. 4 Band structures and DOSs for (a and a′) Sc-doped, (b and b′) C-doped, and (c and c′) Sc/C-codoped TiO_2 (101) surface. The dotted black lines indicate the Fermi level that is set to zero. The solid and dotted red lines indicate the conduction band (CB) position and valence band (VB) position of the pure and doped TiO_2 (101) surface, respectively.

that the host band gap decreased to 2.97 eV and resulted in a red-shift of the absorption edge. Interestingly, the TiO_2 (101) surface became an indirect band gap by doping carbon. Moreover, three impurity states appeared in the band gap, so the minimum energy difference between the CBM and these impurity states was 1.95 eV, which was much smaller than the band gap of the pure TiO_2 (101) surface. It also indicated that those isolated impurity states reduce the excitation energy of the electron transition, resulting in a red-shift of the absorption edge.[51,52] In addition, it could be clearly observed that the three impurity states were mainly contributed by the hybridized energy states between Ti-t_{2g}, Ti-e_g, O-2p, and C-2p orbits (Fig. 4(b′)), which were attributed to the formation of the Ti–C bond and C–O bond for the interstitial C atom. Owing to the asymmetry of the spin-up and spin-down states, a hole state was introduced in the top of VB. Furthermore, the effective masses of the carriers (m_e^* and m_h^*) for the undoped, Sc-doped, C-doped and Sc/C-codoped TiO_2 (101) surfaces have been obtained from parabolic fitting to the CBM and VBM along a specific direction in the reciprocal space. The average effective masses of the photogenerated electrons (holes) in the undoped, Sc-doped, C-doped and Sc/C-codoped systems were about 1.60 (2.94) m_0, 1.55 (3.33) m_0, 1.58 (6.49) m_0 and 1.67 (3.57) m_0, respectively. It is well known that the large difference between m_e^* and m_h^* will further lead to the large difference between the transfer rates of holes and electrons, promoting the separation of photoinduced carriers. The differences of all doped systems were greater than that of the pure TiO_2 (101) surface. This also could explain why all doped systems have higher photocatalytic activity than the undoped surface in Fig. 6.

For the Sc and C codoping (Fig. 4(c) and (c′)), both VBM and CBM significantly decreased with the values of 0.48 eV and 0.52 eV, respectively. It is worth noting that three impurity states were introduced in the band gap located between the VBM and Fermi level. Because the energy difference between the impurity states and the VBM was only 0.49 eV, these impurity states could be seen as shallow acceptor states and promoted the separation of photo-generated electron–hole pairs. The effective band gap was estimated to be 2.52 eV by measuring the minimum energy difference between the impurity states and CBM, which was much smaller than the band gap of the pure TiO_2 (101) surface (2.99 eV), but was greater than that of the C-doped TiO_2 (101) surface. In addition, these impurity states were mainly composed of the O-2p states and slightly contributed by hybridization between the Ti-t_{2g}, Ti-e_g, O-2p and C-2p orbits. The absence of a hole state at the top of VB was attributed to the synergistic effect between the Sc and C impurities.

Table 3 Average Bader charges for the pure and Sc- or/and C-doped TiO_2 (101) surfaces

Model	Ti	O	Sc	C
Pure	+2.25	−1.12	—	—
Sc-doped	+2.27	−1.13	+1.96	—
C-doped	+2.27	−1.15	—	+0.86
Sc/C-codoped	+2.29	−1.15	+1.89	+0.60

The electron density difference in Fig. 5 showed that the charge redistribution mainly occurred around the doping atoms. The electrons migrated between the Ti, O, Sc, and C atoms. In order to explore the charge transfer quantitatively, the average charges of Ti, O, Sc, and C in the pure, C-doped, Sc-doped and Sc/C-codoped surfaces were calculated according to the Bader charges analysis summarized in Table 3.[53] The average charges of the Ti and O atoms in the pure TiO_2 (101) surface were calculated to be +2.25 and −1.12, respectively. After doping, the occupation states of the Ti-3d and O-2p orbital would be affected by the extra electrons or holes from the doping atoms (Sc or C).

The optical absorption spectra (OAS) for the pure and three doped models were calculated by the obtained complex

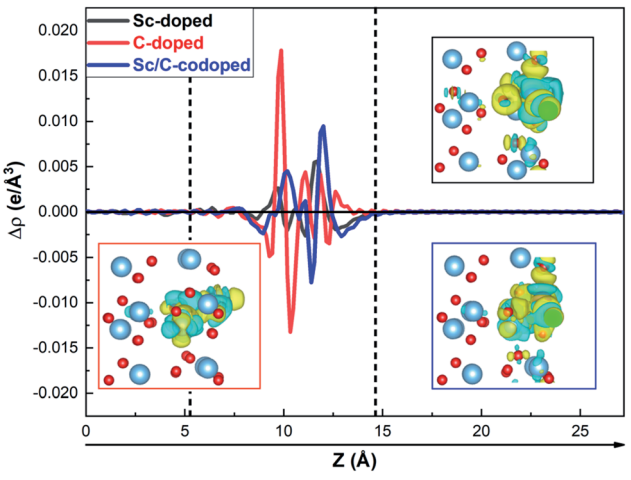

Fig. 5 Planar-averaged electron density difference $\Delta\rho$ for the Sc-doped, C-doped and Sc/C-codoped TiO_2 (101) surfaces. These interpolated maps show the charge density difference between 5.3 eV and 14.6 eV. The yellow and cyan indicate the electron accumulation and depletion, respectively.

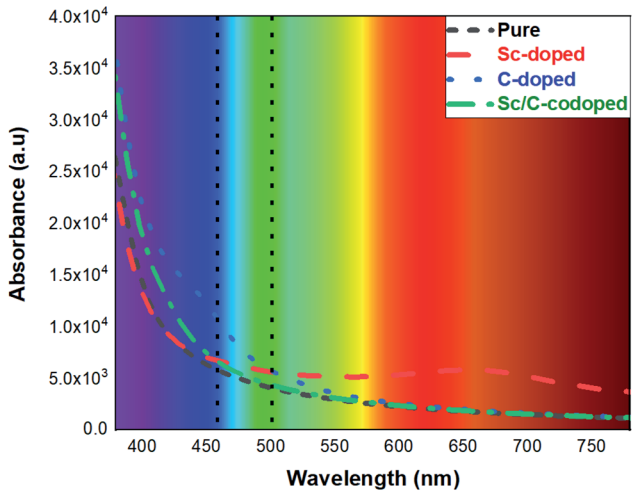

Fig. 6 The optical absorption spectra of pure and doped TiO_2 (101) surfaces in the visible light region.

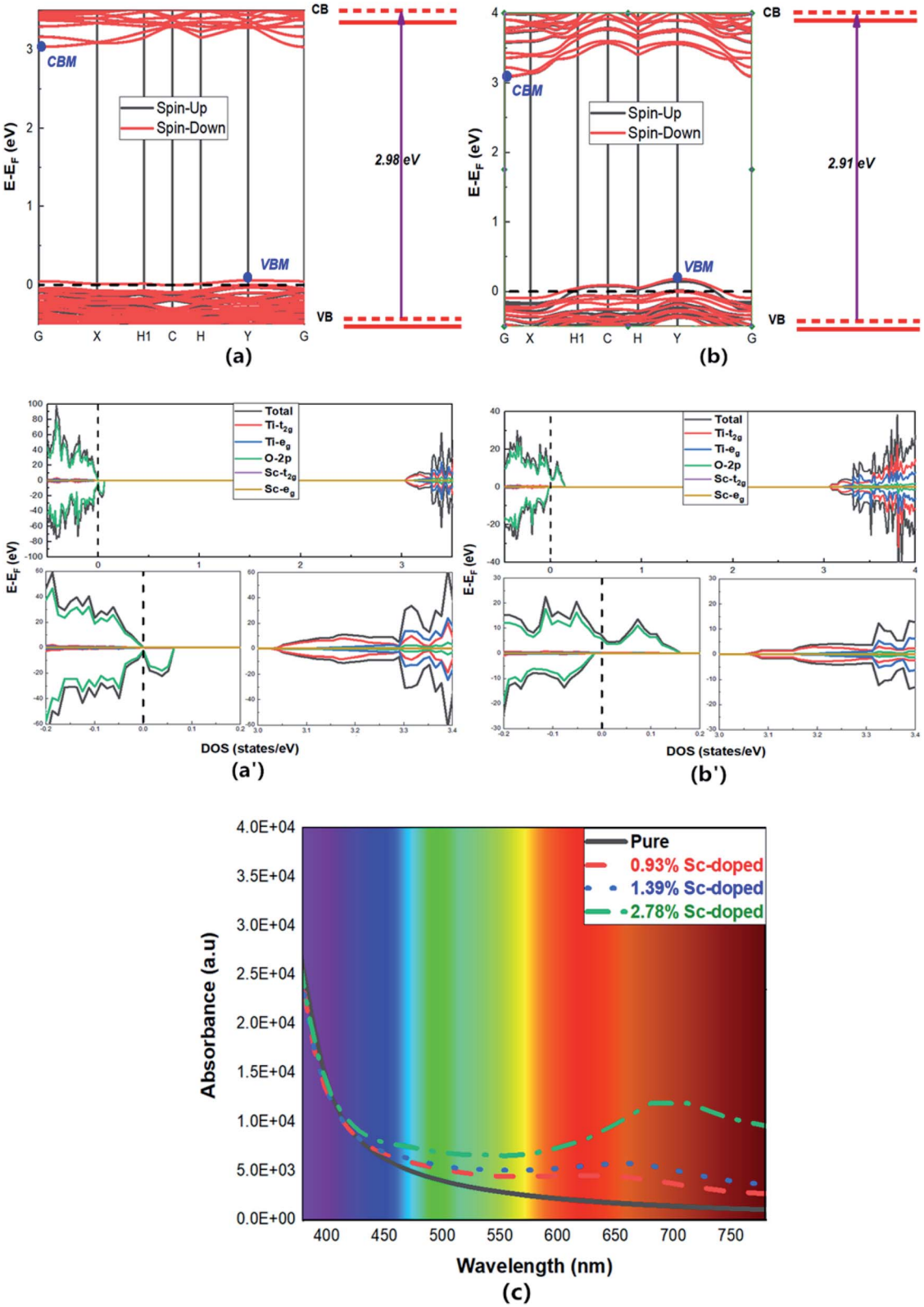

Fig. 7 Band structures, DOSs and optical absorption curves of different impurity concentrations in the Sc-doped TiO_2 (101) surface: (a and a′) Sc: 0.93%; (b and b′) Sc: 2.78%; (c) Sc: all impurity concentrations.

dielectric constant. As shown in Fig. 6, the optical absorption coefficients increased to some extent and the red-shift of the absorption edge could be observed owing to the presence of the impurity states in the band gap after Sc or/and C doping. The OAS in the visible light region could be roughly divided into three parts, high energy zone (380–457 nm), medium energy

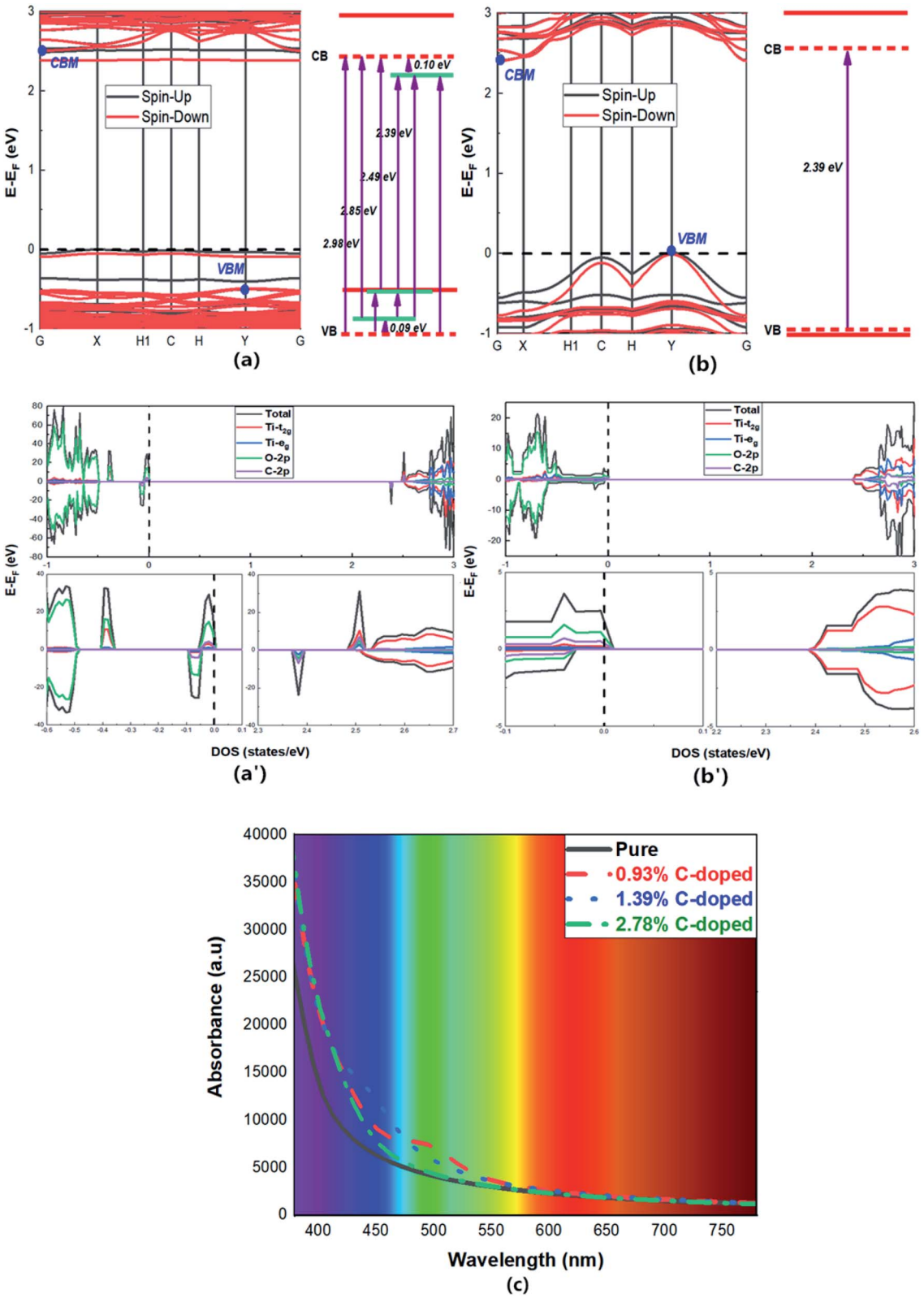

Fig. 8 Band structures, DOSs and optical absorption curves of different impurity concentrations in the C-doped TiO_2 (101) surface: (a and a′) C: 0.93%; (b and b′) C: 2.78%; (c) C: all impurity concentrations.

zone (457–503 nm), and low energy zone (503–780 nm). It is well known that bulk TiO_2 has no response to the visible light. Compared to bulk TiO_2, the absorption edge of the pure TiO_2 (101) surface was extended to the visible light region. The absorption coefficient clearly increased in the medium energy and low energy zones for the Sc-doped TiO_2 (101) surface, which

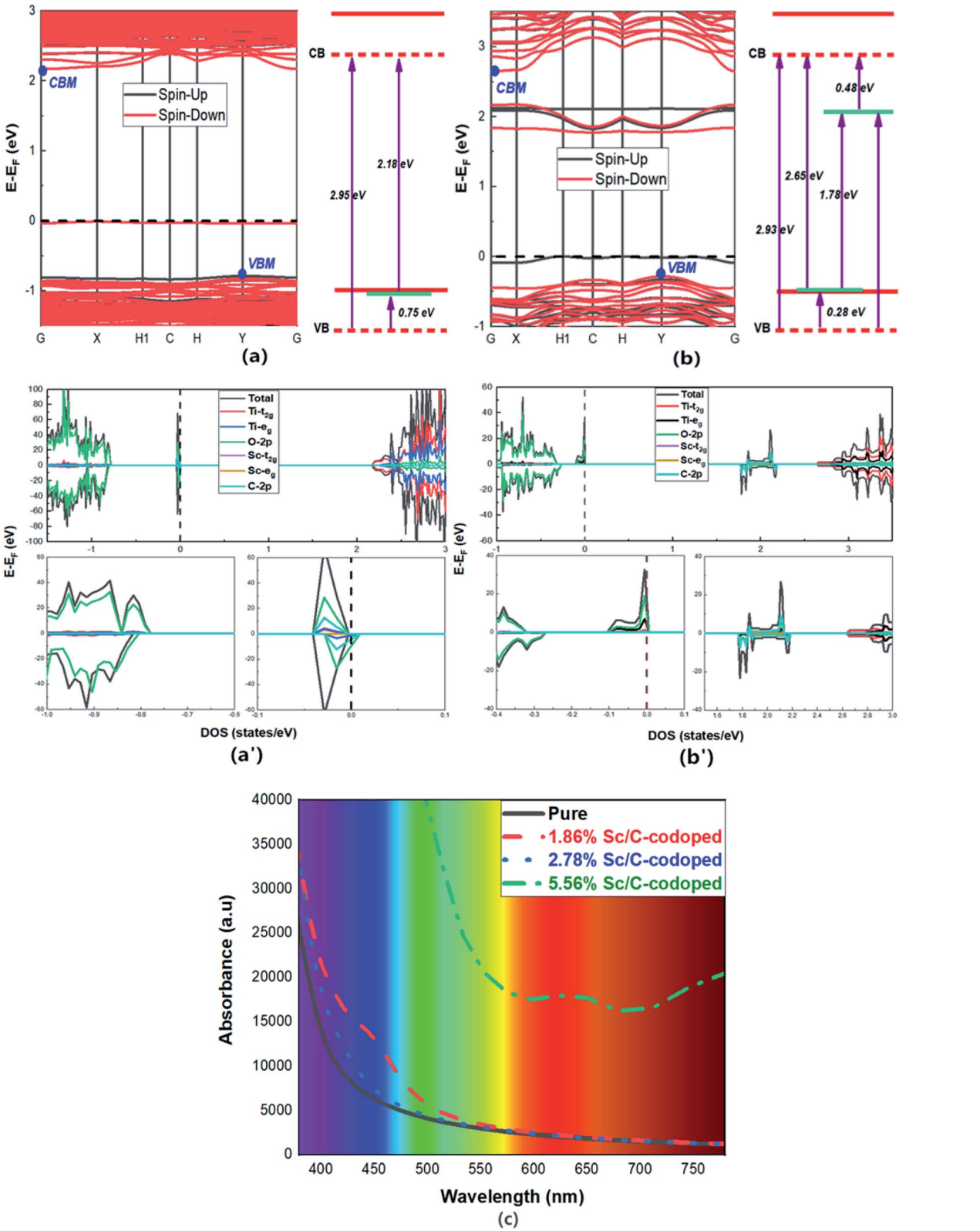

Fig. 9 Band structures, DOSs and optical absorption curves of different impurity concentrations in the Sc/C-codoped TiO_2 (101) surface: (a and a′) Sc/C: 1.86%; (b and b′) Sc/C: 5.56%; (c) Sc/C: all impurity concentrations.

could be mainly ascribed to the reduction of the band gap and the formation of a hole state near the Fermi level. In particular, the excitation energy of the electrons from VB to the empty bands was greatly reduced due to the presence of unoccupied O-2p orbits; thus, the absorption coefficient in the long wavelength range remarkably increased.

For the C-doped TiO_2 (101) surface, the reduction of the host band gap led to a red shift of the absorption edge. The minimum energy difference between CBM and the impurity states was reduced to 1.95 eV, attributed to the appearance of impurity states in the band gap. Thus, the C-doped TiO_2 (101) surface exhibited a stronger absorption coefficient in the medium energy and high energy zones. Nevertheless, the impurity states near the Fermi level were seen as a recombination center, which would restrain the photocatalytic performance. For the Sc/C-codoped surface, the optical absorption had an obvious enhancement in the high energy zone compared to the pure TiO_2 (101) surface because of the introduction of shallow impurity states in the band gap induced by the synergistic effect of the Sc and C atoms. However, its absorption coefficient was less than that of the Sc-doped and C-doped surfaces in the visible light range, which was mainly attributed to a deficiency of empty bands near the Fermi level and large energy difference between CBM and the impurity states, respectively.

3.3 The influences of impurity concentration

The influence of the impurity concentration on the electronic and optical properties of the Sc- or/and C-doped TiO_2 (101) surfaces was investigated through calculating the optical absorption spectra, band structures and DOSs of various impurity concentrations, as shown in Fig. 7–9. It was found that the hole state gradually upshifted into the band gap, and the band gap reduced with increasing Sc concentration for the Sc-doped TiO_2 (101) surface, which resulted in the increase of the light absorption intensity shown in Fig. 7(c). Moreover, a direct–indirect transition for the band gap could be realized when the doping concentration changed from 1.39% (Fig. 4(a) and (a′)) to 0.93% (Fig. 7(a) and (a′)) or 2.78% (Fig. 7(b) and (b′)). Here, the indirect band gap could hinder the carrier recombination.

It is obvious that some shallow impurity states were introduced above VBM and under CBM in the 0.93% C-doped surface (Fig. 8(a) and (a′)), which prompted the separation of the electron–hole pairs. The host band gap for 0.93% doping concentration was almost unchanged compared with the pure model, but the effective band gap derived from the maximum energy difference among the impurity states becomes 2.39 eV. With 1.39% C doping concentration (Fig. 4(b) and (b′)), the impurity states under CBM downshifted toward the Fermi level. Moreover, the effective band gap decreased from 2.39 eV to 1.95 eV, resulting in a red shift of the absorption edge. For the case of 2.78% C doping concentration (Fig. 8(b) and (b′)), the host band gap was reduced to 2.39 eV. Therefore, the absorption coefficient of 2.78% C-doped surface was higher than that of the pure model, but was lower than that of 0.93% and 1.39% C-doped concentration, owing to the absence of shallow impurity states in the band gap (Fig. 8(c)).

The absorption coefficients first decreased and then increased with increasing doping concentration for the Sc/C-codoped surface shown in Fig. 9(c). The factors, the formation of the shallow impurity states in the band gap, empty bands near the Fermi level, and the significantly reduced host band gap (2.95 eV) and effective band gap (2.18 eV) were responsible for the increase of the absorption coefficients in the 1.86% Sc/C-codoped TiO_2 (101) surface (Fig. 9(a) and (a′)). Compared to the 1.86% Sc/C-codoped TiO_2 (101) surface, the absorption coefficient for the 2.78% impurity concentration (Fig. 4(c) and (c′)) clearly decreased, mainly due to the absence of unoccupied states and enlargement of the host band gaps. For the 5.56% Sc/C-doped TiO_2 (101) surface (Fig. 9(b) and (b′)), the host and effective band gaps could be further decreased by about 0.02 eV and 0.4 eV with respect to the 1.86% doping concentration, respectively. Some shallow impurity states were introduced above the VBM and under the CBM, which promoted the effective separation of the photo-excited electron–hole pairs. According to the above analysis, the Sc/C-codoped TiO_2 (101) surface with 5.56% doping concentration was favorable for the generation and separation of electron–hole pairs, leading to the best photocatalytic performance among all doping models in the visible light region in our calculations.

4 Conclusions

In conclusion, the electronic and optical properties of various Sc-doped, C-doped, and Sc/C-codoped TiO_2 (101) surfaces have systematically been studied by first-principles calculations. We found that the Sc@Ti^5 and C@in2 defects were relatively easy to form under both O-rich and Ti-rich conditions. Sc and C impurities could cause apparent lattice deformation in the TiO_2 (101) surface, which may induce a dipole moment and promote the separation of photo-generated electron–hole pairs. With regard to the C-doped surface, the presence of isolated hybridized states in the forbidden gap could effectively lower the excitation energy of the electron transition, and result in a red shift of the absorption edge. For the Sc/C-codoped TiO_2 (101) surface, the optical absorption could be extended in the high energy zone because of some shallow impurity states in the band gap of the TiO_2 (101) surface, which was derived from the synergistic effect between the Sc and C atoms. In addition, it was found that the optical absorption performance could be improved with increasing Sc and C concentration. When the impurity concentration of Sc and C reached up to 5.56% the Sc/C-codoped TiO_2 (101) surface achieved better photocatalytic performance in our calculations, which could be ascribed to the emergence of some shallow impurity states and the introduction of empty bands near the Fermi level.

Conflicts of interest

The authors declare no conflict of interest.

Acknowledgements

This work was supported by the National Natural Science Foundation of China (No. 21763007, 11964004), the Hundred

Talents Program of Guizhou Province (No. QKHPTRC[2016] 5675), and the Program for Innovative Research Team of Guizhou Province (No. QKHPTRC[2020]5023). D. L. acknowledged support of the Natural Science Foundation of Department of Education of Guizhou Province (KY[2020]039). All calculations were performed at Lijiang Cloud Computing Center.

References

1 Y. Lu, W. Yin, K. Peng, K. Wang, Q. Hu, A. Selloni, F. Chen, L. Liu and M. Sui, *Nat. Commun.*, 2018, **9**, 2752.
2 Y. Huang, Y. Jia, R. Hou, Z. Huang, K. Shen, G. Jin and L. Hou, *RSC Adv.*, 2021, **11**, 24172–24182.
3 S. Wang, X. Han, Y. Zhang, N. Tian and T. Ma, *Small Struct.*, 2021, **2**, 2000061.
4 L. Liu, H. Huang, Z. Chen, H. Yu, K. Wang, J. Huang, H. Yu and Y. Zhang, *Angew. Chem., Int. Ed.*, 2021, **60**, 18303–18308.
5 H. Yu, F. Chen, X. Li, H. Huang, Q. Zhang, S. Su, K. Wang, E. Mao, B. Mei, G. Mul, T. Ma and Y. Zhang, *Nat. Commun.*, 2021, **12**, 594.
6 Z. Xiong, H. Wang, N. Xu, H. Li, B. Fang, Y. Zhao, J. Zhang and C. Zheng, *Int. J. Hydrogen Energy*, 2015, **40**, 10049–10062.
7 B. Fang, Y. Xing, A. Bonakdarpour, S. Zhang and D.-P. Wilkinson, *ACS Sustainable Chem. Eng.*, 2015, **3**, 2381–2388.
8 J. Zhang, M. Deng, F. Ren, Y. Wu and Y. Wang, *RSC Adv.*, 2016, **6**, 12290–12297.
9 Z. Wang, B. Xiao, Z. Lin, Y. Xu, Y. Lin, F. Meng, Q. Zhang, L. Gu, B. Fang, S. Guo and W. Zhong, *Angew. Chem., Int. Ed.*, 2021, DOI: 10.1002/anie.202110335.
10 W. Zhong, B. Xiao, Z. Lin, Z. Wang, L. Huang, S. Shen, Q. Zhang and L. Gu, *Adv. Mater.*, 2021, **33**, 202007894.
11 S. Shen, Z. Lin, K. Song, Z. Wang, L. Huang, L. Yan, F. Meng, Q. Zhang, L. Gu and W. Zhong, *Angew. Chem.*, 2021, **60**, 12360.
12 Z. Lin, B. Xiao, Z. Wang, W. Tao, S. Shen, L. Huang, J. Zhang, F. Meng, Q. Zhang, L. Gu and W. Zhong, *Adv. Funct. Mater.*, 2021, **31**, 2102321.
13 Z. Wang, Z. Lin, J. Deng, S. Shen, F. Meng, J. Zhang, Q. Zhang, W. Zhong and L. Gu, *Adv. Energy Mater.*, 2021, **11**, 2003023.
14 H. Tang, F. Levy, H. Berger and P. E. Schmid, *Phys. Rev. B: Condens. Matter Mater. Phys.*, 1995, **52**, 7771.
15 N. Swaleha, K. Wasi, K. Shakeel, H. Shahid and A. Abid, *J. Lumin.*, 2019, **205**, 406–416.
16 G. Han, J. Kim, K. J. Kim, H. Lee and Y. M. Kim, *Appl. Surf. Sci.*, 2020, **507**, 144916.
17 V. Thongpool, A. Phunpueok, S. Jaiyen and T. Sornkwan, *Results Phys.*, 2020, **16**, 102948–102959.
18 S. Li, Z. Wang, Y. Yang, J. Li and C. Jin, *Micro Nano Lett.*, 2020, **15**, 226–229.
19 K.-R. Anju, T. Radika, R.-J. Ramalignam and H.-A. Al-Lohedan, *Optik*, 2018, **165**, 408–415.
20 Y. Lin, Z. Jiang, C. Zhu, X. Hu, X. Zhang, H. Zhu, J. Fan and S. Lin, *J. Mater. Chem. A*, 2013, **1**, 4516–4524.
21 G.-W. Lin, Y.-H. Huang, W. Tseng and F.-H. Lu, *Ceram. Int.*, 2019, **45**, 22506–22512.
22 J. Lu, Y. Dai, M. Guo, L. Yu, K. Lai and B. Huang, *Appl. Phys. Lett.*, 2012, **100**, 102114.
23 R. Fagan, D.-E. McCormack, S. Hinder and S.-C. Pillai, *Mater. Des.*, 2016, **96**, 44–53.
24 P.-W. Dunne, C.-L. Starkey, A.-S. Munn, M. Sikder, O. Luebben, I. Shvets and E.-H. Lester, *J. Environ. Chem. Eng.*, 2016, **4**, 2665–2670.
25 C. Byrne, L. Moran, D. Hermosilla, N. Merayo, Á. Blanco, S. Rhatigan, S. Hinder, P. Ganguly, M. Nolan and S. Pillai, *Appl. Catal., B*, 2019, **246**, 266–276.
26 T. Raguram and K.-S. Rajni, *Appl. Phys. A: Mater. Sci. Process.*, 2019, **125**, 288.
27 H. Liu, Y. Wu and J. Zhang, *ACS Appl. Mater. Interfaces*, 2011, **3**, 1757–1764.
28 J. Cai, W. Xin, G. Liu, D. Lin and D. Zhu, *Mater. Res.*, 2016, **19**, 401–407.
29 C. Morgade and G. Cabeza, *Comput. Mater. Sci.*, 2016, **111**, 513–524.
30 X. Li, J. Shi, H. Chen, R. Wan, C. Leng, S. Chen and Y. Lei, *Comput. Mater. Sci.*, 2017, **129**, 295–303.
31 H. Chen, X. Li and R. Wan, *Comput. Condens. Matter*, 2017, **13**, 16–28.
32 M. Nasir, J. Lei, W. Iqbal and J. Zhang, *Appl. Surf. Sci.*, 2016, **364**, 446–454.
33 G. Kresse and J. Furthmüller, *Comput. Mater. Sci.*, 1996, **6**, 15–50.
34 G. Kresse and D. Joubert, *Phys. Rev. B: Condens. Matter Mater. Phys.*, 1999, **59**, 1758.
35 J. Perdew, K. Burke and M. Ernzerhof, *Phys. Rev. Lett.*, 1996, **77**, 3865.
36 M. Fox, *Optical Properties of Solids*, Oxford University Press, Oxford, 2001.
37 J. K. Burdett, T. Hughbanks, G. J. Miller, J. W. Richardson and J. V. Smith, *J. Am. Chem. Soc.*, 1987, **109**, 3639–3646.
38 Y. Ortega, N. C. Hernandez, E. Menéndez-Proupin, J. Graciani and J. F. Sanz, *Phys. Chem. Chem. Phys.*, 2011, **13**, 11340–11350.
39 V. Wang, N. Xu, J. C. Liu, G. Tang and W. Geng, *Comput. Phys. Commun.*, 2021, **267**, 108033.
40 M. Lazzeri, A. Vittadini and A. Selloni, *Phys. Rev. B: Condens. Matter Mater. Phys.*, 2001, **63**, 155409.
41 H. Liu, M. Zhao, Y. Lei, C. Pan and W. Xiao, *Comput. Mater. Sci.*, 2012, **51**, 389–395.
42 P. Knauth and H. L. Tuller, *J. Appl. Phys.*, 1999, **85**, 897.
43 Y. Hu, Y. Pan, Z. Wang, T. Lin, Y. Gao, B. Luo, H. Hu, F. Fan, G. Liu and L. Wang, *Nat. Commun.*, 2020, **11**, 2129.
44 D.-X. Li, R.-Q. Li, X.-M. Qin and W.-J. Yan, *Phys. Lett. A*, 2019, **383**, 2679–2828.
45 D. Ren, H. Li and X. Cheng, *Solid State Commun.*, 2015, **223**, 54–59.
46 N. Umezawa and J. Ye, *Phys. Chem. Chem. Phys.*, 2012, **14**, 5924–5934.
47 H. Tang, H. Berger, P. Schmid and F. Lévy, *Solid State Commun.*, 1993, **87**, 847–850.
48 C. Jin, Y. Dai, W. Wei, X. Ma, M. Li and B. Huang, *Appl. Surf. Sci.*, 2017, **426**, 639–646.

49 A. Latini, C. Cavallo, F.-K. Aldibaja, D. Gozzi, D. Carta, A. Corrias, L. Lazzarini and G. Salviati, *J. Phys. Chem. C*, 2013, **117**, 25276–25289.
50 K. Xiong, Q. Zheng, Z. Cheng and P. Liu, *Eur. Phys. J. B*, 2020, **93**, 201.
51 P. Wahnon, J. C. Conesa, P. Palacios, R. Lucena, I. Aguilera, Y. Seminovski and F. Fresno, *Phys. Chem. Chem. Phys.*, 2011, **13**, 20401–20407.
52 R. Lucena, I. Aguilera, P. Palacios, P. Wahnón and J. C. Conesa, *Chem. Mater.*, 2008, **20**, 5125–5127.
53 W. Tang, E. Sanville and G. Henkelman, *J. Phys.: Condens. Matter*, 2009, **21**, 084204.